Full-spectrum periodic nonlinear Fourier transform optical communication through solving the Riemann-Hilbert problem

Morteza Kamalian-Kopae, Anastasiia Vasylchenkova, Dmitry Shepelsky, Jaroslaw E. Prilepsky, and Sergei K. Turitsyn, *Fellow, OSA*

***Abstract*—In this work, for the first time, a full-spectrum periodic nonlinear Fourier transform (NFT) based communication system with the inverse transformation at the transmitter performed by using the solution of Riemann-Hilbert problem (RHP), is proposed and studied. The entire control over the nonlinear spectrum rendered by our technique, where we operate with two qualitatively different components of this spectrum represented, correspondingly, in terms of the main spectrum and the phases, allows us to design a time-domain signal tailored to the characteristics of the transmission channel. In the heart of our system is the RHP-based signal processing utilised to generate the time-domain signal from the modulated nonlinear spectrum. This type of NFT processing leads to a computational complexity that scales linearly with the number of time-domain samples, and we can process signal samples in parallel. In this paper, we suggest the way of getting an exactly periodic signal through the correctly formulated RHP, and present evidence of the analogy between band-limited (in ordinary Fourier sense) signals and finite-band (in RHP sense) signals. Also, for the first time, we explain how to modulate the phases of individual periodic nonlinear modes. The performance of our transmission system is evaluated through numerical simulations in terms of bit error rate and Q^2-factor dependencies on the transmission distance and power, and the results demonstrate the good potential of the approach.**

***Index Terms*—Fibre-optic communications, coherent communications, nonlinear Fourier transform, inverse scattering, Riemann-Hilbert problem.**

I. Introduction

Since the advent of inverse scattering transform [1] and NFT-based signal processing and eigenvalue communication dating back to the pioneering work of Hasegawa and Nyu [2], the NFT has attracted a great deal of interest and was intensively studied in the context of optical communications (see e.g. [3–6] and references therein). Due to the trivial and uncoupled evolution of the nonlinear spectrum (NS) components as the signal propagates through the nonlinear fibre for the nonlinear Fourier modes attributed to decaying profiles, the NFT can be efficiently utilised in overcoming nonlinear signal distortions. However, there are many limitations in practical implementation of the "conventional" NFT, where the signal is assumed to vanish in time at some point [4, 7–10]. One of them is that for the computations involved in the NFT processing to be sufficiently accurate, the signal support should be long enough and account for the dispersion-induced memory. This requirement alone entails two problems: (i) growing numerical errors associated with our dealing with long pulses [11], and also the transmission degradation due to the joint action of dispersive signal spreading and noise [6, 12], and (ii) a high computational complexity due to the necessity to process a lot of samples consecutively [9]. The fastest numerical routine proposed in [13] offers the $O(N\log^2 N)$ complexity to produce an N-sample signal from its continuous NS, not taking into account the possible presence of discrete NS eigenvalues (solitary spectrum). The performance of those computational methods also deteriorates with the growth of signal energy, thus requiring that some higher values of N are used to get a smaller sample size and attain the acceptable accuracy of the result [14, 15].

As an alternative to the "conventional" NFT paradigm dealing with rapidly-decaying signals applied to optical communications, we can use periodically-extended signals — the approach well developed for linear optical channels [16]. For instance, one can append signal with a cyclic prefix, similar to the coherent optical OFDM format, and then still use the NFT-type approach for processing [7, 17, 18]. Such an opportunity was, perhaps, first mentioned in [14] and studied theoretically for an exemplary setup in [19], and a simple system based on the periodic nonlinear modes modulation has been recently demonstrated experimentally [20]. Aside from a row of other advantages listed in the previous works [7, 21], the periodic NFT (PNFT) not only provides an explicit control over the signal duration, but can also reduce noticeably the required processing window at the receiver, as we do not have to process the dispersion-induced memory [7, 8, 17, 21, 22]. The latter fact can make a substantial difference for long-haul transmission, insofar as using the PNFT we are to process only one period of the signal [7, 22].

The main challenge for the PNFT utilisation in communications has so far been to find a flexible method to construct a periodic signal from its NS, i.e. the inverse PNFT, and to be able to retrieve the encoded data back

M. Kamalian, A. Vasylchenkova, J. E. Prilepsky and S. K. Turitsyn are with the Aston Institute of Photonic Technologies, Aston University, Birmingham, B4 7ET, UK.

D. Shepelsky is with B.Verkin Institute for Low Temperature Physics and Engineering, 47 Nauky Ave., Kharkiv, 61103, Ukraine and V.N.Karazin Kharkiv National University, 4 Svobody Square, Kharkiv, 61022, Ukraine.

e-mail: m.kamalian-kopae1@aston.ac.uk (M. Kamalian-Kopae)

at the receiver. The conventional description of the NS for a periodic signal includes [14]: a static part, i.e. the so-called main spectrum, and a dynamical part, called the auxiliary spectrum. The latter characterises the evolution of the signal as it propagates through the fibre. However, the difficulty here is that the evolution of the auxiliary NS part is governed by a set of coupled *nonlinear* differential equations [14], such that when using them directly we *effectively loose the very advantage of the NFT-based methods*. Even though these equations can be turned into linear relations using an algebro-geometric construction called the Abel map [23], the conventional algebro-geometric approach to the inverse PNFT, i.e. to the construction of a (quasi-) periodic signal from its main and transformed auxiliary NS, entails the evaluation of computationally-expensive functions – the multidimensional Riemann theta-functions [23]. While this problem can be avoided in some special cases [8, 18], where only a few signal parameters are used for the modulation, this general drawback hampers signal-generation flexibility and restrains system's throughput, as the signal processing based on that method with multiple data carries is unlikely to become technically feasible due to its high complexity.

At the same time, there exists a general approach to calculating the inverse PNFT, which is based on the formalism of Riemann-Hilbert problems (RHP). A RHP itself is posed as the task of finding the solution of a special analytic factorisation problem defined inside the nonlinear Fourier domain [3, 21, 24]. Note, when using this approach, the computational complexity of the numerical inverse transformation scales linearly with the number of temporal samples, each sample can be processed independently, and the computations for the whole set of our signal samples can be carried out in parallel. Although some other NFT methods do also have this property [25], their usage has not been that popular in communications. Importantly, within the RHP approach we do not have to deal with the auxiliary spectrum, which is replaced by the *phases* of nonlinear modes, whose evolution turn out to be linear.

In the first proof-of-concept configuration proposed by us in [21, 24], we did not incorporate phases and employed only two degrees of freedom per signal, associated with the main spectrum, that were used there for the modulation and carrying our data. In the present work, we develop the RHP approach further, designing the system that employs for the modulation of all available parameters attributed to a periodic finite-band solution to nonlinear Schrödinger equation (NLSE). Our new signal modulation method is capable of carrying multiple phase-shift keying (PSK) symbols via modulating the spectral parameters complementary to the main spectrum – the phases (which substitute the conventional auxiliary spectrum, as mentioned above), while we still can control the signal characteristics by manipulating the main spectrum values.

In our work we deal with the signal propagation down the single-mode fibre, operating with single polarisation. The signal evolution is described by the (normalised) NLSE:

$$i q_z + q_{tt} + 2|q|^2 q = 0, \tag{1}$$

which is widely considered as a principal master leading-order model governing the path-averaged evolution of the slow-varying optical field envelope $q(t,z)$ in a fibre with anomalous dispersion (z plays the role of the distance along the fibre, while t is the retarded time variable [26, 27]). In our approach we will be dealing with the special class of NLSE solutions: the so-called finite-band periodic solutions [23, 28]. These solutions can be deemed of as the nonlinear analogue of a function containing a finite number of Fourier harmonics, i.e. they comprise a finite number of extended nonlinear modes. It also means that we have a finite number of the NS quantities fully characterising our signal. To model the spontaneous emission noise emerging in the optical fibre links due to the amplification, in the evaluation of the transmission system's performance, Sec. V-C, we will include the additive white Gaussian noise term in the r.h.s. of (1). The explicit normalisation for the communication systems employing single-mode fibres can be found in, e.g., Ref. [4].

The rest of the paper is organised as follows. In Sec. II we present the basic introductory information regarding the PNFT, with some reference to general NFT theory and specific peculiarities of the approach used in our current work. In Sec. III we discuss the structure of the communication systems based on the NFT utilisation. A comprehensive description of the pair of inverse and direct transforms is presented in Secs. IV-A and IV-C, respectively. Sec. IV-B addresses the periodicity of the signal and explains how we can adjust the desirable period. The resulting signal parameters and their links with the NS structure are discussed in Sec. V-A. The transmission simulation results for various signal power and propagation distances are presented in Sec. V-C. Sec. V-B is devoted to the limitations, arising from the numerical accuracy. After the conclusive section, Appendix A presents the relationship between various RHPs involved in the RHP formalism of the inverse problem, and two methods of getting the periodic solution are discussed in Appendix B.

Throughout this text we use l.h.s and r.h.s acronyms to point the left-hand-side and right-hand-side of equations.

II. Periodic nonlinear Fourier transform

The NLSE, belonging to the class of integrable nonlinear equations, can be represented as the compatibility condition for the so-called Lax pair, the pair of 2×2 linear operators [3]. The first entry of the Lax pair consists of the Zakharov-Shabat system, the core part of the NFT decomposition. It is written for an auxiliary function $\mathbf{\Phi}(t,z,\lambda)$ as

$$\mathbf{\Phi}_t = \begin{bmatrix} -i\lambda & q(t,z) \\ -q^*(t,z) & i\lambda \end{bmatrix} \mathbf{\Phi}, \tag{2}$$

where the complex spectral parameter λ entering this equation can be understood as a nonlinear analogue of frequency. Given $q(t,z)$ as a function of t (for a fixed z), the

associated NS can be determined in terms of the solution of (2) with appropriate boundary conditions. Finding the corresponding NS via solving the Zakharov-Shabat problem constitutes the direct part of the NFT. The second equation from the Lax pair,

$$\mathbf{\Phi}_z = \mathbf{R}(t,z,\lambda)\mathbf{\Phi}, \tag{3}$$

with

$$\mathbf{R}(\lambda,t,z) = \begin{bmatrix} i|q|^2 - 2i\lambda^2 & 2\lambda q + iq_t \\ -2\lambda q^* + iq_t^* & -i|q|^2 - 2i\lambda^2 \end{bmatrix}, \tag{4}$$

defines the z-evolution of NS components.

The idea of NFT can be understood as the parametrisation of the solutions to the NLSE by a set of parameters, which we call the NS. In solving an integrable equation, the NLSE in our case, by means of the NFT, the Zakharov-Shabat problem (2) is first solved. The solutions are used to define the set of appropriate spectral characteristics (i.e. the NS) associated to the given initial data $q(t,0)$, where, for simplicity, we take that initial condition at $z=0$. In view of the second Lax equation, we can find the evolved NS at some desired point z. Finally, one obtains the solution $q(t,z)$ of the nonlinear equation for an arbitrary z by solving the inverse problem: given the evolved spectral data, retrieve the "potential" $q(t,z)$ that enters the first Lax equation.

Depending on the boundary conditions for the NLSE, the appropriate set of NS parameters can acquire different forms [4], see also the discussion in our previous work [21]. Generally, the NFT operation can be understood as a change of variables from $q(t,z)$ to the NS parameters. For a vanishing signal (decaying sufficiently fast as t tends to infinity), the "standard NS" consists of a continuous function defined on the real line of λ-plane, plus some discrete complex numbers associated to a set of complex-valued eigenvalues. All these NS parameters can be found straightforwardly by considering the Zakharov-Shabat problem (2). The evolution of these "standard" parameters is simple and uncoupled. For the NLSE with periodic boundary conditions, all the spectral information is, in principle, contained in the monodromy matrix [7, 14], which is made of special solutions of the same Zakharov-Shabat problem (2), see more explanations below in Sec. IV-C. However, the question of how we can pick out a part (or a special form) of these data that can serve as an "appropriate NS", is less straightforward. First, there must be a one-to-one unambiguous correspondence between the NS and a two-dimensional solution of the NLSE: every cross-section of the solution at fixed $z=z_0$ has to be uniquely associated to a "cross-section" of the NS at $z=z_0$. Second, in the sense of "change of variables", one would like to have the following properties: the NS parameters should evolve with z in a simple (preferably, linear) way, and there should be a (numerically) efficient procedure based on the chosen set of NS parameters to solve the inverse problem. The same requirements are actually imposed for the NFT applications in optical communications [4].

Turning now to the problem in hand, the "conventional" NS for the NLSE periodic in t-variable, consists of zeros of certain functions, which are static, and called main spectrum. These functions are expressed in terms of the entries of the monodromy matrix. Another part of the NS, the dynamical part, is called auxiliary spectrum and is also determined by the monodromy matrix. However, such an NS parametrisation suffers from the fact that, while the main spectrum is invariant under the evolution along z, the dynamical part – the auxiliary spectrum – evolves with z in a complicated, nonlinear manner. This property undermines the very reason of using the NFT in optical communications.

In view of the arguments above, for the communication system considered in our current work, we use a different PNFT NS parametrisation: similarly to the conventional approach, our set of spectral parameters comprise an ordinary main spectrum invariant under evolution along z, but the dynamical part is represented by a set of real-valued phases that substitute the auxiliary spectrum; the meaning of this naming convention will become clear from the expressions given in Sec. IV-A. In this paper, we will be modulating special periodic solutions of NLSE, in which the number of the main spectrum points, as same as the number of phases, is finite; denoting this number by $\mathcal{N}+1$, we have in total $3\mathcal{N}+3$ real degrees of freedom that can be used in our transmission system. In the context of communication, this number relates to the amount of information that can be carried by such a signal. We shall call such solutions "finite-band", although the names "finite-gap" or "finite-genus" are also used in the literature.

To sum up, the NS for both (quasi)-periodic and vanishing signals can be split into the dynamical part and z-invariant part, as our signal propagates through the fibre. The invariant part of the NS of periodic signal is the main spectrum, somewhat similar to the eigenvalues emerging in the NFT of a vanishing signal. The dynamical part for a periodic signal can be given by the phases emerging somewhat like the phases of spectral amplitudes corresponding of the discrete and continuous spectra in vanishing case: the dynamics of each nonlinear modes for both cases is uncoupled and linear. In order to solve the inverse problem, in our paper we use the RHP formalism; the details are given in Sec. IV-A. The phases also enter naturally into RHP-based processing method: the important advantage of this approach is that it allows us to gain the linear evolution (in z) of the phases.

On the other hand, within our approach here we face the problem of providing periodicity (in t) of the NLSE solution obtained as a result of solving the inverse problem. Indeed, our inverse problem results in a finite-band solution, which is not, in general, periodic, but only quasi-periodic in t. Then, within our approach here, the problem of ensuring the periodicity can be reduced to that of providing the commensurability of all partial "frequencies" attributed to each nonlinear mode. This question is explicitly addressed in Sec. IV-B below. Finally, the direct problem stage in our approach consists in calculating the phases from the monodromy matrix associated to our encoded signal; an overview of this stage is presented in Sec. IV-C.

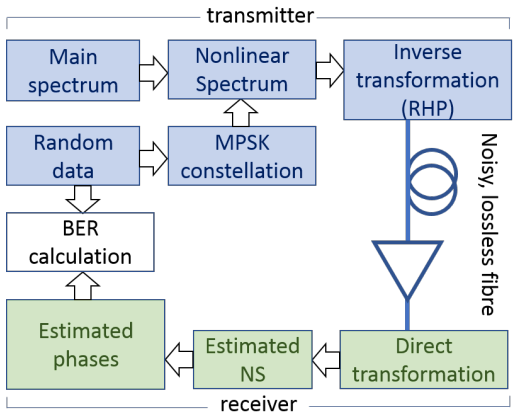

Fig. 1: The schematics of the studied communication system: on the Tx side the main processing is performed by means of solution of the RHP (Sec. IV-A), while the Rx processing is done by the use of direct NFT (Sec. IV-C).

Finally in this section, we note that the constituents of NS do not necessarily have a direct physically-meaningful counterparting quantities in the space-time domain, as the meaning of the NS is that it is a special nonlinear parametrisation of our solution. Such a correspondence can be established for very simple situations (e.g. a single soliton or a single extended periodic mode) which are, however, not that interesting for the communication applications, where we need as many available data carriers as possible.

III. A PNFT-BASED COMMUNICATION SYSTEM

Having parametrised the periodic solutions of NLSE, we can now compose a wide class of signals by adjusting the particular NS structure. On top of that, due to its simple linear evolution with z, as opposed to the complicated, nonlinear evolution of the signal in space-time domain, the NS emerges as a convenient data-bearer in a nonlinear optical fibre system, such that nonlinear frequency division multiplexing concept [3] can be built up.

In a communication system, the ultimate goal is to transfer information carried by a signal from a transmitter, through a medium, to a receiver. The information is mapped on some parameters of signal at the transmitter, and then we need to recovered it from the received distorted signal. Within the nonlinear frequency division multiplexing we use the NS as the set of signal parameters that carry the information, such that either whole NS or some of its parts are modulated with a random stream of symbols. As it is usually the case, there are some characteristics of the signal which are predefined based on the requirements of the link such as signal bandwidth, power, etc. Since the NS uniquely determines the signal, fixing these characteristics will lead to a loss of some degrees of freedom available for modulation. As will be shown later, in our case most of the communication-related characteristics of signals are related to the main spectrum. Therefore, in this work we specifically design the main spectrum of our signals to adjust its characteristics, and modulate the remaining phases to transfer our data. This means that for the signal containing $\mathcal{N}+1$ nonlinear modes (an $\mathcal{N}+1$-band solution), out of $3\times(\mathcal{N}+1)$ total degrees of freedom participating in the NS, we employ $2\times(\mathcal{N}+1)$ parameters to control signal's periodicity, duration and power, and only modulate the remaining $\mathcal{N}+1$ phases.

The communication system considered in our work, schematically shown in Fig. 1, is not principally different from other typical NFT-based setups. In our case, we use the specially structured main spectrum to manipulate signal power, bandwidth and period, as well as the periodicity property itself. This main spectrum is known by the receiver and is constructed through a procedure which will be explained later. Then, the random bit stream is mapped to the MPSK symbols, the values of which are taken as the values of the phases attributed to each nonlinear mode. Along the main spectrum, this set of phases makes up the full NS. A signal with the chosen modulated NS is then generated through the inverse transformation using the RHP, and sent to the fibre. Undergone linear and nonlinear distortion in addition to the amplifier spontaneous emission (ASE) noise, the signal is received at the Rx. The NS of the signal is then calculated via the direct transformation using the Zakharov-Shabat problem. The first (invariant) part of the NS, i.e. the main spectrum, is already known by the receiver, but its calculated values can be used to further equalise the signal. The dynamical NS part contains the transmitted random data in the form of phases. These phases are then recovered from the monodromy matrix, and the encoded data are eventually retrieved.

The direct and inverse transformation stages are performed through using some existing numerical routines [29–31], and the details of their functioning together with the setting used will follow. The numerical accuracy of these calculations play a significant role in the performance of our system, which leads to the main limitation source of such communication systems, so that we address the related effects separately. Finally we note that numerous equalisation schemes can be used to further remove the residual impacts of fibre and additive noise in the nonlinear Fourier domain in order to improve the quality of transmissions. A few examples including linear equalisers and machine learning methods in application to the different NFT-based systems, can be found in [32–37].

IV. NFT COMPUTATIONS: INVERSE AND DIRECT TRANSFORMS FOR PERIODIC SOLUTIONS

This section lays down the procedures to calculate the NS of a periodic signal and also to construct the time-domain profile of a finite-band solution to the NLSE corresponding to a given NS.

A. Inverse transform: constructing a finite-band NLSE solution via the solution of a RHP

In our communication system, we start with the inverse transformation stage of the NFT at the transmitter side,

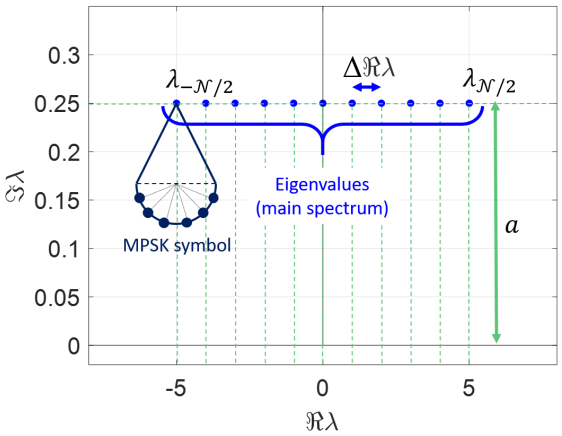

Fig. 2: The schematic structure of the NS for a periodic finite-gap signal. In order to ensure the periodicity, the points of the main spectrum (shown as equidistant points) are to be slightly readjusted. The global signal parameters are mainly influenced by the main spectrum ($\Delta\Re\lambda$ influences period while $\Im\lambda \equiv a$ determines power and bandwidth). Since at the receiver we retrieve the phases modulo π (see Sec. IV-C), they are depicted as half-circles associated with each point of the main spectrum.

$z=0$, employing the (modulated) parameters of NS as data carriers. The output of the inverse transform generates the respective time-domain profile [4].There are two general approaches to construct a solution of the NLSE starting from its NS. The first one is based on solving the famous Gelfand-Levitan-Marchenko equation [38], which is a linear integral equation formulated in the time domain, with input data constructed from the (linear) Fourier transform of the NS. The second approach, which is the one we will discuss here, is to solve an associated RHP formulated in the complex plane of the spectral parameter λ [21, 28, 30, 39].

In a nutshell, a RHP consists in finding an analytic function (which can be a vector- or matrix-valued) in the complex plane, defined off a given curve, knowing its behaviour at the infinity and how its value changes when one approaches that curve from either side. In our case, this change is expressed in terms of a multiplicative jump: as a matrix-valued function crosses a curve, it is multiplied by a 2×2 matrix, the so-called jump matrix.

Then, if the jump matrix depends also on t and z (as parameters) in an explicit way, the solution of the RHP (which depends on t and z as well), evaluated as $\lambda\to\infty$, produces a solution to the nonlinear equation in question, the NLSE in the case considered.

Let the NS consist of $\mathcal{N}+1$ complex parameters $\{\lambda_j\}_{j=0}^{\mathcal{N}}$, the main spectrum, and $\mathcal{N}+1$ real parameters $\{\phi_j\}_{j=0}^{\mathcal{N}}$, the phases, see Fig. 2. We associate to this set (i) the (oriented) contour Γ being the union of non-intersecting curves, $\Gamma = \cup_{j=0}^{\mathcal{N}}\Gamma_j$, where $\Gamma_j = \widehat{(\lambda_j,\lambda_j^*)}$ is the particular curve connecting λ_j and its complex conjugate, and (ii) the 2×2-valued functions depending on our phases:

$$\mathbf{J}_j(t,z,\lambda) = \begin{bmatrix} 0 & ie^{-i(\phi_j+2\lambda t+4\lambda^2 z)} \\ ie^{i(\phi_j+2\lambda t+4\lambda^2 z)} & 0 \end{bmatrix}, \quad \lambda\in\Gamma_j, \tag{5}$$

with $j=0,\dots,\mathcal{N}$. Then we formulate the RHP (in fact, a family of RHP parametrised by t and z): given $\{\lambda_j\}_{j=0}^{\mathcal{N}}$ and $\{\phi_j\}_{j=0}^{\mathcal{N}}$, find a piece-wise analytic, 2×2-valued function $\mathbf{\Psi}(t,z,\lambda)$ satisfying the following conditions:

$$\begin{aligned} &\mathbf{\Psi}^+(t,z,\lambda) = \mathbf{\Psi}^-(t,z,\lambda)\mathbf{J}_j(t,z,\lambda), \qquad \lambda\in\Gamma_j, \\ &\mathbf{\Psi}(t,z,\lambda) = \mathbf{I} + O\left(\lambda^{-1}\right), \qquad \lambda\to\infty, \end{aligned} \tag{6}$$

where $\mathbf{I}$ is the 2×2 identity matrix and the superscripts $\pm$ denote the limiting values of $\mathbf{\Psi}^-(t,z,\lambda)$ as λ approaches Γ_j from the different sides in accordance with the orientation of Γ_j.

Having solved the RHP (5), (6), the solution $q(t,z)$ of the NLSE is given by the expression

$$q(t,z) = 2i\,\mathbf{\Psi}_1^{1,2}(t,z),$$

where the superscript $\{1,2\}$ stands for the corresponding matrix entry, and the quantity $\mathbf{\Psi}_1(t,z)$ is defined through the limiting relation:

$$\mathbf{\Psi}_1(t,z) = \lim_{\lambda\to\infty}\lambda\left(\mathbf{\Psi}(t,z,\lambda)-\mathbf{I}\right).$$

By construction, $q(t,z)$ is a finite-band solution of the NLSE: the spectrum of the differential operator involved in (2) and considered as acting in $L_2(\mathbb{R})$ consists of $\mathcal{N}+1$ curves connecting λ_j (being the main spectrum points) with λ_j^*. The associated function $\mathbf{\Phi} := \mathbf{\Psi}e^{-(i\lambda t+2i\lambda^2 z)\sigma_3}$, where $\sigma_3 = \left(\begin{smallmatrix}1 & 0\\ 0 & -1\end{smallmatrix}\right)$, solves the both equations, (2) and (3), of the Lax pair; it is the so-called (planar) Baker-Akhiezer function of the NLSE [23, 28].

A finite-band solution is, in general, quasi-periodic in t, but not necessarily periodic [23]. In order to control the behaviour of $q(t,z)$ as the function of t and z, it is convenient to use the flexibility of the RHP representation of $q(t,z)$: the same $q(t,z)$ can be represented in terms of different RHPs. Particularly, $q(t,z)$ can be represented in terms of the solution of a RHP, whose jump matrices (across each Γ_j) are independent of λ, but are linearly dependent on t and z, see [28] and [21, Appendix B, Eqs. (23)–(26)]:

$$q(t,z) = 2i\hat{\mathbf{\Phi}}_1^{1,2}(t,z)\,e^{2if_0 t+2ig_0 z}, \tag{7}$$

where $\hat{\mathbf{\Phi}}_1^{1,2}(t,z)$ is the respective matrix element in the large-λ limit expansion,

$$\hat{\mathbf{\Phi}}(t,z,\lambda) = \mathbf{I} + \hat{\mathbf{\Phi}}_1(t,z)/\lambda + \dots,$$

as $\lambda\to\infty$, and $\hat{\mathbf{\Phi}}(t,z,\lambda)$ is the solution to the following RHP:

$$\begin{aligned} &\hat{\mathbf{\Phi}}^+(t,z,\lambda) = \hat{\mathbf{\Phi}}^-(t,z,\lambda)\hat{\mathbf{J}}_j(t,z), \qquad \lambda\in\Gamma_j \\ &\hat{\mathbf{\Phi}}(t,z,\lambda) = \mathbf{I} + O(\lambda^{-1}), \qquad \lambda\to\infty, \end{aligned} \tag{8}$$

with the jump matrix:

$$\hat{\mathbf{J}}_j(t,z)=\begin{bmatrix}0 & ie^{-i(\phi_j+C_j^f t+C_j^g z)}\\ ie^{-i(\phi_j+C_j^f t+C_j^g z)} & 0\end{bmatrix},\quad \lambda\in\Gamma_j, \tag{9}$$

where $j=0,\dots,\mathcal{N}$. Here the "frequencies" C_j^f, "wave numbers" C_j^g, and the constants f_0 and g_0 are determined by the points λ_j only, see Appendix A.

The jumps $\hat{\mathbf{J}}_j(t,z)$ have a linear dependence on t and z demonstrating explicitly the (quasi) periodic behaviour of $\hat{\mathbf{\Phi}}$ and, thus, of $q(t,z)$. Particularly, if the "frequencies" $\{C_0^f,\dots,C_{\mathcal{N}}^f,f_0\}$ turn out to be commensurable (meaning all be integer multiples of a common value), then $q(t,z)$ is periodic with respect to t.

This approach allows us to effectively separate the influence of main spectrum points λ_j and phases ϕ_j, so one can use the phases ϕ_j for the data modulation while leaving the set of λ_j to manipulate signal characteristics.

The numerical methods for the RHP solutions are available, see Refs. [29, 30]. The RHP, including our case here, can be solved for each point in time t and distance z independently (same as the Darboux transform). This leads to a crucial advantage of the RHP-(P)NFT nonlinear signal processing method over the methods widely used in the conventional NFT communication framework: we can now make up a long signal with many samples without losing the numerical accuracy due to the high energy of such a signal. Note that the latter is a significant challenge when dealing with ordinary NFT signal processing [9].

B. Periodicity of the resulting finite-band signal

To make sure that at the receiver we are able to find the NS, we need to guarantee the periodicity of the solution while generating it at the transmitter. As we mentioned, in order to arrive at the periodic NLSE solutions when performing the inverse part of the NFT, it is sufficient to require all frequencies $\{C_0^f,\dots,C_{\mathcal{N}}^f,f_0\}$ to be commensurable. These frequencies are determined uniquely by the composition of main spectrum points λ_j through (21) and (22), see Appendix A. In particular, we can chose such a set of λ_j as to have $C_j^f=j-\mathcal{N}/2-1$ and $f_0=0$. The condition $f_0=0$ can be guaranteed by imposing, in the general case, the constraint on C_j^f:

$$\sum_{j=1}^{\mathcal{N}} C_j^f\int_{\Gamma_j}\frac{\xi^{\mathcal{N}}d\xi}{w^+(\xi)}=-i\pi\sum_{j=0}^{\mathcal{N}}(\lambda_j+\lambda_j^*). \tag{10}$$

Then, Eq. (21) complemented by (10), can be viewed as a system of $\mathcal{N}+1$ complex-valued nonlinear equations with respect to λ_j: given $\{C_j^f\}_{j=0}^{\mathcal{N}}$, find $\mathcal{N}+1$ complex parameters λ_j entering the coefficients of that system. In order to get the set of λ_j corresponding to the desired periodic solution, we employ an iterative approach starting from $\{\lambda_j\}$ located equidistantly, as in the case of a signal with infinitesimal power, see Appendix B-A.

An alternative way of finding a periodic solutions relies on computing the main spectrum attributed to some arbitrary periodic function $\hat{q}(t)$ having the desired parameters, see Appendix B-B. After that, the resulting main spectrum (if we have arrived at a finite-band case, i.e. one has a finite number of λ_j) attributed to the chosen $\hat{q}(t)$, can be used as the main spectrum of our new signal, where the phases are modulated with the data to transmit. However we do not employ this method in our current paper.

C. Direct transform and computation of phases ϕ_j

Calculating the NS (the main spectrum points λ_j and the phases ϕ_j) from a signal $q(t)=q(t,z=L)$, with L being the transmission distance, at the receiver, constitutes the direct part of the PNFT. Recall that in the periodic case, all the spectral information associated with q is contained in the 2×2 monodromy matrix $\mathbf{M}(\lambda)=\mathbf{M}(\lambda,z)$, see the details in [7, 14]. The monodromy matrix is defined as $\mathbf{M}(\lambda,z)=\mathbf{\Phi}(T,z,\lambda)$, where $\mathbf{\Phi}(t,z,\lambda)$ is the solution of the Zakharov-Shabat equation (2) satisfying the initial condition $\mathbf{\Phi}(0,z,\lambda)=\mathbf{I}$. Thus, we need to determine our NS, $\{\lambda_j\}$ and $\{\phi_j\}$, from $\mathbf{M}(\lambda,L)$. Below we briefly describe this procedure. (i) $\{\lambda_j\}_{j=0}^{\mathcal{N}}$ can be found as simple zeros of the equation involving the trace of $\mathbf{M}(\lambda)$, which is independent of z:

$$\left(\mathbf{M}^{1,1}+\mathbf{M}^{2,2}\right)^2-4=\mathrm{Tr}\,[\mathbf{M}]^2-4=0; \tag{11}$$

(ii) the determination of phases $\{\phi_j\}_{j=0}^{\mathcal{N}}$ involves the off-diagonal elements of $\mathbf{M}$: $\mathbf{M}^{1,2}$ and $\mathbf{M}^{2,1}$, evaluated at Γ_j, and the points of the *auxiliary spectrum* [7, 14, 40], which are either double zeros of $\mathbf{M}^{1,2}$, or simple zeros of $\mathbf{M}^{1,2}$ that do not coincide with double zeros of the l.h.s. of Eq. (11). Namely, introducing the function

$$P(\lambda)=\log\left(\sqrt{-\frac{\mathbf{M}^{1,2}(\lambda)}{\mathbf{M}^{2,1}(\lambda)}}\prod_{j=1}^{\mathcal{N}}\frac{\lambda-\mu_j^*}{\lambda-\mu_j}\right), \tag{12}$$

where μ_j are the points of auxiliary spectrum, the phases $\{\phi_j\}_{j=0}^{\mathcal{N}}$ are uniquely determined from the system of $\mathcal{N}+1$ linear equations ($\phi=[\phi_0,\dots,\phi_{\mathcal{N}}]^T$):

$$\mathbf{K}\phi=B. \tag{13}$$

Here the entries of the $(\mathcal{N}+1)\times(\mathcal{N}+1)$ matrix $\mathbf{K}[m,j]=K_{mj}$ are defined by

$$K_{mj}=\int_{\Gamma_j}\frac{x^m dx}{w^+(x)},\quad j,m=0,\cdots,\mathcal{N}, \tag{14}$$

and the components B_m of the r.h.s. vector B are as follows

$$B_m=-i\sum_{j=0}^{\mathcal{N}}\int_{\Gamma_j}\frac{P(x)x^m}{w^+(x)}dx,\quad m=0,\dots,\mathcal{N}, \tag{15}$$

where $w^+(\xi)$ designates the limiting values of the function

$$w(\lambda)=\prod_{j=0}^{\mathcal{N}}\sqrt{(\lambda-\lambda_j)(\lambda-\lambda_j^*)} \tag{16}$$

on a particular curve Γ_j, choosing the branch with the cuts along Γ_j and fixed by the condition $w(\lambda)\sim\lambda^{\mathcal{N}+1}$ as $\lambda\to\infty$. The algorithm (12)-(16) for determining ϕ_j can be justified by using a series of deformations of RHP associated with the NLSE with periodic q; the mathematical details, having

a certain analogy with the case of the Korteweg-de Vries equation [41], will be presented elsewhere.

Ignoring the choice of the branch of the square root in the definition of P, Eq. (12), the phases are reconstructed by modulo π, such that the phase's two values different by π cannot be distinguished. Consequently, in our current work we use the halved MPSK constellations, as shown in Fig. 2, assuming that $\phi_j \in (0,\pi)$, and leave the question of using the full 2π phase interval for future studies.

Finally, the linear dependence on z of the phases in (9) allows retrieving the transmitted phase values $\phi_j(z=0)$ from $\phi_j(z=L)$ calculated, via solving the direct part of the NLS, at the receiver side:

$$\phi_j(z=L) = \phi_j(z=0) + C_j^g L - 2g_0 L. \tag{17}$$

Notice that in [21], only the main spectrum of the NS was used to carry the data, and the system employed the z-invariance of the main spectrum points. However, the limited number of degrees of freedom and the problem of enforcing the periodicity for our signals suggest using phases as the data carriers while keeping the main spectrum fixed, in analogy with what was proposed for ordinary solitons [5]. In this way, we choose the main spectrum points to have the desired signal characteristics such as power and period. Then, the MPSK symbols are mapped to the phases entering the jump matrices, Eq. (5) or (9). The generated signal with modulated phases is then sent to the fibre, and the phase content of the NS, $\phi_j(z=L)$, is calculated at the receiver using the direct PNFT and the procedure described above. Finally, the initial encoded phase values $\phi_j(z=0)$ are retrieved using Eq. (17).

V. Numerical Simulations and results

In this section, we numerically investigate the different aspects and quality characteristics of the communication system based on PNFT, and analyse the properties of our specific phase-modulated signals in the space-time domain. We also address numerical accuracy and some limitations in performing the PNFT computations and signal design.

A. Signal characteristics determined by the main spectrum

In the current study, we consider the specifically structured main spectrum: we position its values almost equidistantly over the straight line parallel to the real λ-plane axis, thus keeping the same the imaginary part for all points, as sketched in Fig. 2. This choice makes our numerical calculations simple without loss of generality, as we are only interested in modulating the phases.

We notice that within this section we provide the signal parameters for the normalised signal $q(t,z)$, which is a solution to the normalised NLSE (1). In order to get the dimensional values of respective quantities, one should perform a backward renormalisation of the NLSE. The normalisation is defined by a single normalisation parameter that can be, let say, the time normalisation scale T_s [4]. The normalisation for our system here is not different from that for other NFT-based approaches. The main spectrum structure chosen in our work allows us to manipulate the signal parameters, such that we can the desirable values of power, while phases attributed to each nonlinear mode will bear the encoded information. The three examples of a signal generated via the RHP solution, where each signal has three points in its main spectrum, $\{-0.37-0.33i, 0.33i, 0.37-0.33i\}$, with different phases attributed to each nonlinear mode, are shown in Fig. 3. When computing the signal profiles in time domain, starting from the main spectrum of the type shown in Fig. 2, we observed that the signal power mainly depends on the imaginary part of the main NS points. As it is seen from Fig. 4, the picture is nearly uniform in the abscissa direction for four main spectra with various number of points, $\mathcal{N} = 4, 6, 8, 10$, except for the region of very small inter-point distances $\Delta\Re\lambda \lesssim 0.5$.

The signal linear bandwidth, depicted in Fig. 5, reveals the same dependency, being predominantly dependent on $\Im\lambda$ aside, again, from the low inter-point distance region. It is necessary to note that the linear bandwidth, as a result of a linear Fourier transform of the signal, is not an invariant parameter of the signal and can vary as the signal propagates through the fibre. The numerically obtained signal bandwidth shown in Fig. 5, depicts the dependency of the signal bandwidth on the main spectrum at $z=0$.

However, we note that some further systematic investigation is necessary to accurately attribute the signal bandwidth and power values to the main spectrum structure. We noticed that at higher signal powers the signal bandwidth appeared to also depend on the imaginary part of the spectrum only. However, this may be the result of numerical errors occurring due to the two following effects. First, at higher powers, our numerical errors associated with the RHP computation generally rise. The second possible explanation is that at small $\Delta\Re\lambda$, the signal period and, therefore, its whole duration (including cyclic prefix) is larger, see Fig. 6, such that for a fixed number of modes $\mathcal{N}$ we get a less accurate numerical result due to larger Δt value. The signal period, on the other hand, seems to only depend on the spacing between the main spectrum points $\Delta\Re\lambda$, Fig. 6.

In our particular case, in order to get a specific signal period from the NS of the form given in Fig. 2, we choose the main spectrum points as to get the following values of the frequencies: $C_j^f = j - \mathcal{N}/2 - 1$. Finding the appropriate main spectrum is done through a procedure explained in Appendix B. Setting the values of C_j^fs introduces the additional constraint on the λ_j locus by linking the corresponding $\Delta\Re\lambda$ and $\Im\lambda$, leaving, hence, only $\Im\lambda$ for our signal power manipulation. As it is observed from Fig. 7, by increasing the imaginary part, we get a higher signal power. However, to keep the signal period constant, we need to slightly reduce the spacing between the main spectrum points, $\Delta\Re\lambda$. This means that the relations derived in Appendix B are only valid for low power signals. We also studied the power deviation for the signals, when generating the signals with different phases ϕ_j, while maintaining the main NS

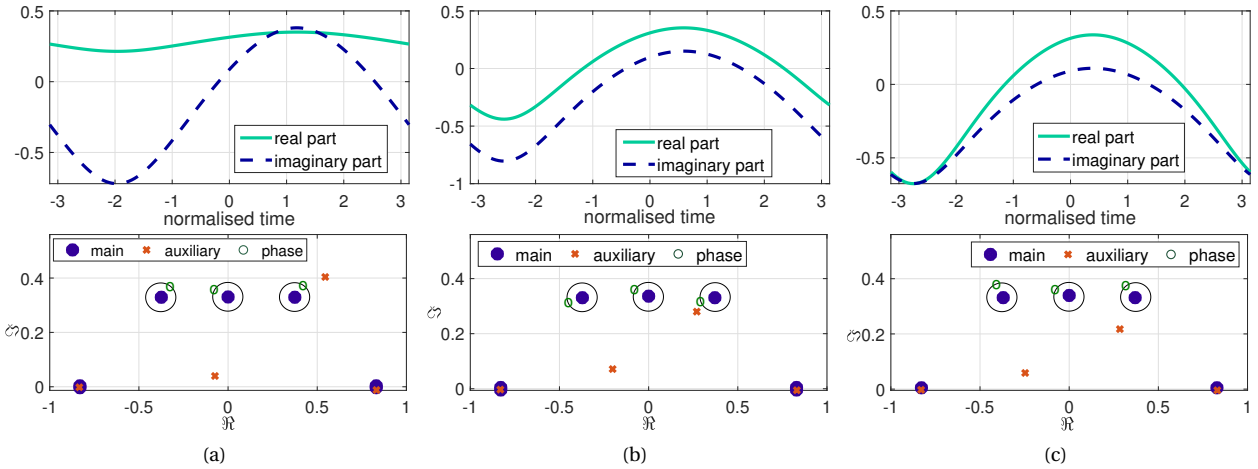

Fig. 3: Three examples of the generated (according to (7)–(9)) 3-band signals with common main spectrum $\lambda = \{-0.37 - 0.33i, 0.33i, 0.37 - 0.33i\}$ and different phases in Eq. (9) set to (a) $\phi = \{\frac{3\pi}{8}, \frac{7\pi}{8}, \frac{3\pi}{8}\}$, (b) $\phi = \{\frac{9\pi}{8}, \frac{7\pi}{8}, \frac{9\pi}{8}\}$, and (c) $\phi = \{\frac{5\pi}{8}, \frac{7\pi}{8}, \frac{5\pi}{8}\}$. The red crosses and blue points are calculated candidates to the auxiliary and main spectral points respectively, retrieved when solving the direct problem, see Subsec. IV-C; those close to the real axis correspond to double zeros of Eq. (11) and thus do not represent actual spectral points. The top plots show the real and imaginary part of the signal over one normalised period 2π and the bottom plots show the respective NS structures.

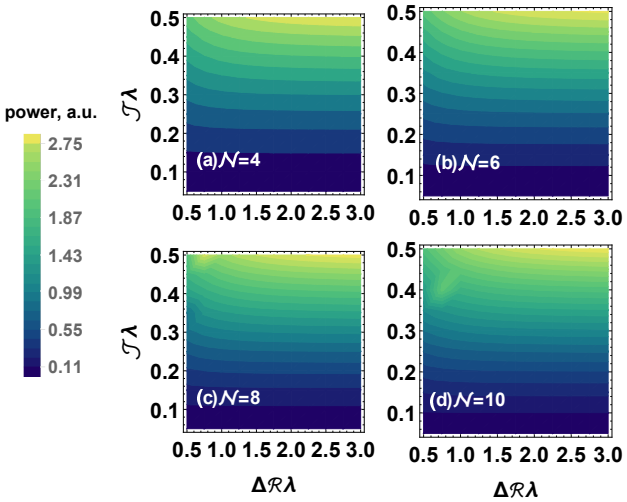

Fig. 4: The signal power as a function of the main NS structure: inter-point distance $\Delta\Re\lambda$ and common imaginary part $\Im\lambda$ (see Fig. 2), for different number of nonlinear modes. As mentioned, the signal power is mainly defined by the imaginary part.

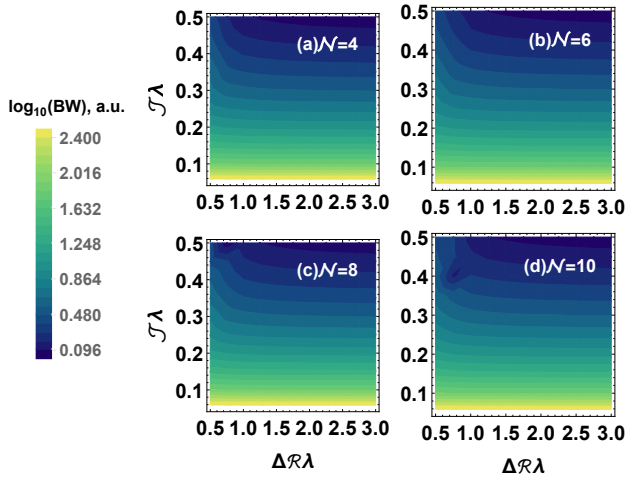

Fig. 5: The signal bandwidth as a function of the main NS structure: inter-point distance $\Delta\Re\lambda$ and common imaginary part $\Im\lambda$ (see Fig. 2), for different number of nonlinear modes. As mentioned, the signal power is mainly defined by the imaginary part.

unchanged. From Fig. 8 we inferred that the signal power changes negligibly, and its deviation is most noticeable for the higher imaginary part of main spectrum points (i.e. for the high signal power). To obtain Fig. 8, many random realisations of phases with a uniform distribution are used and the standard deviation of the obtained signal power for each $\Delta\Re\lambda$ and $\Im\lambda$ point is calculated. This small deviation value makes it evident that it is the main spectrum that mostly determines the signal power for our specific mains spectrum structure. We note here that within the proposed configuration, the signal period and bandwidth are linearly related to the smallest real part of the main spectrum points (here $\Delta\Re\lambda$) and its inverse, respectively. This, in fact, puts a constraint on the time-bandwidth product of the generated signal. In turn, the value of the time-bandwidth product is related to the spectral efficiency of the communication system: getting the larger number of data-carrying signal's degrees of freedom per a time-X-frequency unit means the better use of available resources. To increase the spectral efficiency for our configuration here, one needs to include more data-carrying NS points while keeping $\Delta\Re\lambda$ and $\mathcal{N}\Delta\Re\lambda$ fixed.

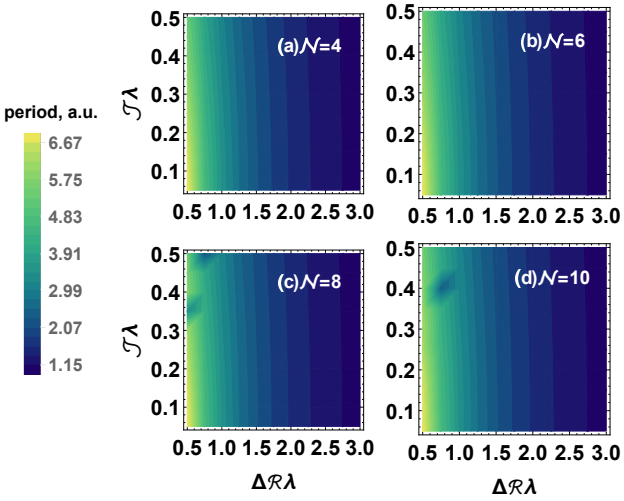

Fig. 6: The signal period as a function of the main NS structure: inter-point distance $\Delta\Re\lambda$ and common imaginary part $\Im\lambda$ (see Fig. 2), for different number of nonlinear modes. As mentioned, the signal power is mainly defined by the real parts spacing.

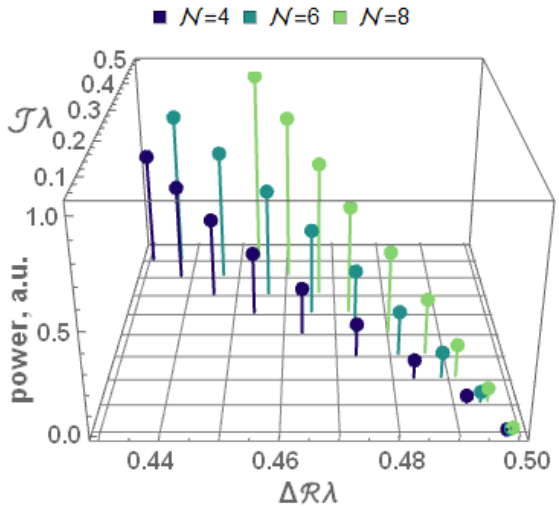

Fig. 7: The signal power as a function of the main NS structure inter-point distance $\Delta\Re\lambda$ and common imaginary part $\Im\lambda$ (see Fig. 2), for different number of nonlinear modes, along the lines in the complex plane of λ, keeping the signal period constant.

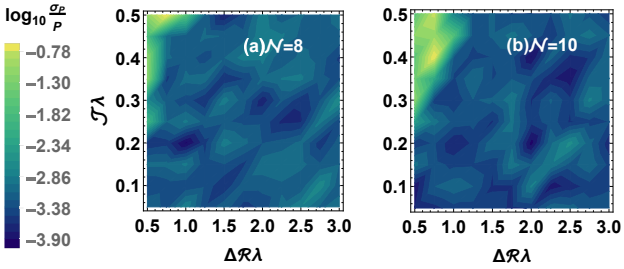

Fig. 8: The relative signal power deviation (power's standard deviation σ_P) over the power value P itself as a function of the main NS structure inter-point distance $\Delta\Re\lambda$ and common imaginary part $\Im\lambda$ (see Fig. 2), for different number of nonlinear modes. The deviation is sufficiently small to conclude that the power is mainly determined by the main spectrum.

B. Accuracy and limitations of the numerical routines

The discussion related to the computational complexity can be divided into two parts, referring to the direct and inverse transformation stages, respectively. In our work, the direct transformation comprises the calculation of monodromy matrix (we did it here by using the normalised Ablowitz-Ladik algorithm of Ref. [14]). Using the numerically obtained monodromy matrix, we then find the main and auxiliary spectra. In addition to these calculations, we need to find the phases carrying our transmitted data, the procedure which entails the numerical evaluation of integrals in Eq. (15) and the solution of the small-size linear ordinary equation, Eq. (13). The latter calls for $\mathcal{N}+1$ evaluations of the argument function over the whole nonlinear spectrum $\mathcal{N}$ cuts, which amounts to $O(\mathcal{N}N_c)$ evaluations of the ratio in Eq. (15), where N_c is the total number of points used to represent the otherwise continuous cuts in the complex λ-plane.

The most demanding part of the inverse transformation stage giving us the time-domain profile, is to solve the RHP. The computational complexity of calculating the value of the signal at each point in time and distance via the numerical RHP solution is of the order $O(N_c \log N_c)$. Here we assume that the discretisation points are uniformly distributed over the cuts. We note that when considering the specific structure of the cuts, the uniform grid might not necessarily be the best option, and some more efficient strategies for the RHP cuts discretisation may exist. In fact, our numerical simulations show a marginal impact of changing N_c on the accuracy of calculations after a certain limiting $\Delta\Im\lambda$ (i.e. the spectral resolution) value, the step between the discretisation points in our cuts. On the other hand, increasing the number of temporal samples, i.e. diminishing the sample value Δt, has a greater impact on the numerical accuracy of the direct and inverse transformations and on the overall performance of resulting communication system. The quality of back-to-back phase computation for our recovering the values of randomly modulated phases ϕ_j in Eq. (9), is shown in Fig. 9 in terms of the Q^2-factor density plot vs $\Delta\Im\lambda$ and Δt. The back-to-back procedure consists of the inverse and direct transformations and accounts for the combined errors produced by both of them together.

The signal power is directly influenced by the imaginary part of the main spectrum and, as discussed in Sec. V-A, is almost independent of phases. Therefore, in the current setting, when we keep the imaginary part of all the eigenvalues in the main spectrum the same and equal to a, see Eq. (26) and Fig. 2, the higher-power signals are obtained by increasing the value of a. We generally mention two limitations for increasing the signal power up to an arbitrary level. The first one is the numerical error ensued from the direct transform stage (see [9, 14]), and the second comes from the inverse transform stage by worsening the spectral resolution, $\Delta\Im\lambda$, see Fig. 9. To explain the latter, note that as signal power gets higher by our raising the imaginary part of the main spectrum, a fixed number of points representing

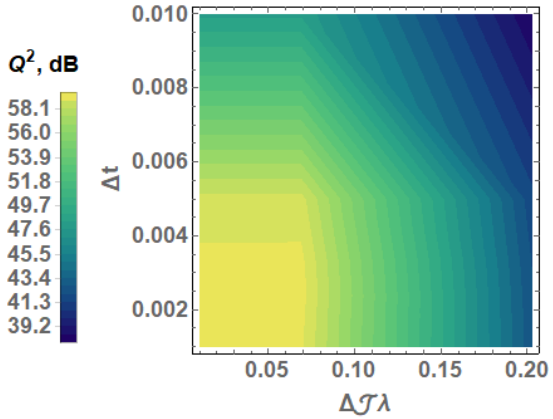

Fig. 9: The Q^2-factor (defined from EVM) of the B2B calculation of phases ϕ_j, embedded into the signal. The signal is generated via the RHP solution for the 15-cuts NS (see Fig. 2). Q^2 is computed as the function of the cut sampling step $\Delta\Im\lambda$ for the vertical cuts, and time sampling step Δt.

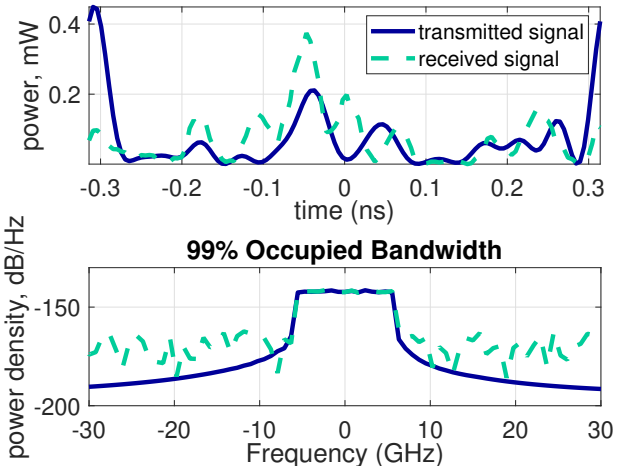

Fig. 10: Example of the transmitted and received signal carrying 15 8-PSK symbols over a link of length 1080 km.

the cuts leads to larger $\Delta\Im\lambda$, which, in turn, gives rise to less accurate numerical results. The other constraint is related to our approach of finding the appropriate main spectrum that guarantees the periodicity of the signal, see Sec. B. As the signal power increases due to our raising the a value in Eq. (26), the search for the numerical solutions of Eq. (26) becomes more difficult and less accurate.

As for the signal bandwidth, another numerical limitation is due to the fact that increasing the bandwidth (while keeping the signal duration fixed) is done by increasing the number of cuts in the main spectrum. Therefore, finding appropriate main spectrum entails solving a system of nonlinear equations with more unknown values, which, in turn, makes solving Eq. (21) numerically more difficult in the general case.

C. Simulation results for a PNFT-based communication system

As an example, to show the noise tolerance and also the fibre impact on the NS of a periodic signal and, as a consequence, on the performance of the PNFT-based communication system with the RHP processing, in our study here we use the signal with the main spectrum structure as in Fig. 2.

In our system, we map the MPSK symbols ($M = 8$) to the phases of a 15-band NLSE solution. The resulting time-domain signal is sent to a fibre link containing 13 80 km long spans, the total transmission distance being 1040 km. The diagram showing the different blocks of our communication system is given in Fig. 1. An ideal distributed Raman amplification (i.e. the zero gain-loss profile) is assumed and SMF parameters of $\beta_2 = -21$ ps^2/km, and $\gamma = 1.3$ W^{-1} km^{-1} are used in the simulation runs. The presence of ASE noise is taken into account by adding the noise term to the r.h.s. of the NLSE. The noise spectral density is calculated as $N_{ASE} = \alpha L \hbar\nu_s K_T$, with fibre loss $\alpha = 0.2$ dB/km^{-1}, $L = 80$ km span length, $\hbar\nu_s$ being the photon energy, and $K_T \approx 1.13$. The number of time samples in a single signal (containing 15 MPSK symbols), i.e. per one period, is 64. Each signal is then cyclically extended in time to the value of the dispersion-induced channel memory at 1040 km according to the linear channel model. However, as we have observed from our simulations, a smaller cyclic prefix can also preclude the effect of inter-symbol interference due to the essentially nonlinear dynamics of our signal. Each PNFT signal, containing 15 8-PSK symbols, consists of 64 time-domain samples at the sampling frequency of 66 GHz (i.e. the time normalisation parameter of $T_s = 0.2$ ns). This leads to a signal duration of ≈ 1.9 ns. Thus we have the baudrate (for MPSK symbols) of 7.94 Gbaud or ≈ 23.7 Gb/s. This signal duration includes the cyclic prefix which is equal to one signal period, and this gives us a useful signal duration of ≈ 0.95 ns. Note that according to the linear dispersive estimations the prefix duration should be much longer. As mentioned earlier, one of the advantages of the PNFT is the smaller processing window at the receiver. At the receiver only one period of signal (here it means just 64 samples) needs to be processed as opposed to the conventional NFT where the whole extended duration (here 128 samples) should be considered. An example of a signal carrying 15 MPSK symbols before adding a cyclic extension and the received signal after removing the cyclic extension is shown in Fig. 10.

The cyclic-prefix-appended signals are then cascaded to form a batch of several consecutive signals. To calculate each Q^2-factor and BER value, 2^8 of such batches were used. The BER is directly calculated by counting the mismatches between the transmitted and received bit streams. Increasing the number of samples improves the performance for both cases of noisy and noiseless transmissions but it has limited impact when noise is the dominant factor in deteriorating the performance—low power region. In the high power areas, increasing the number of samples improves the performance of the noisy transmission but this improvement diminishes as the number of samples grows, similar behaviour for a PNFT communication system based on modulating the main spectrum can be found

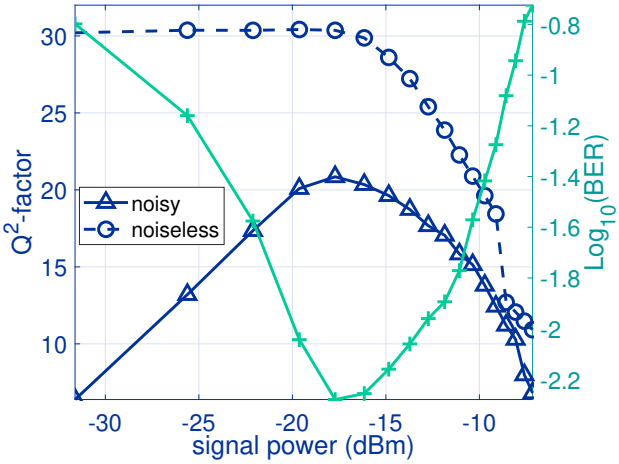

Fig. 11: The Q^2-factor (defined from EVM) and BER versus the signal power after 1040 km transmission. The optimum is achieved at $P = -17$ dBm. The dashed line represents the Q^2-factor for a noiseless transmission which indicates the numerical error as the main contributing factor in performance degradation for higher powers.

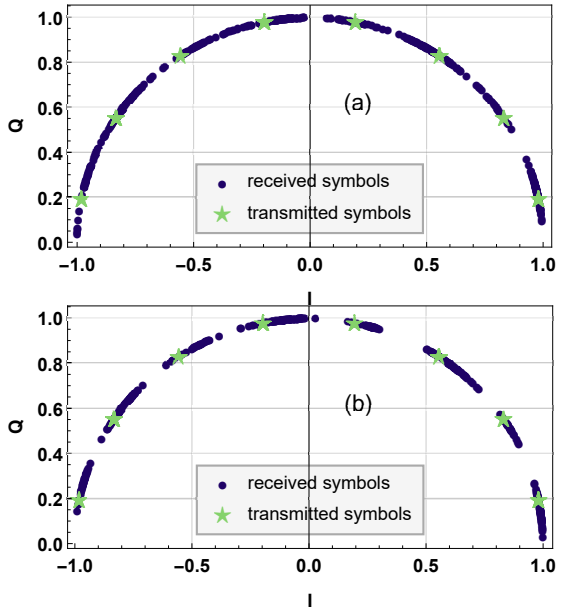

Fig. 12: The received phase constellation after 1000 km transmission of an 8PSK auxiliary spectrum modulated signal at signal power a) $P = -6$ dBm, and b) $P = -17$ dBm.

in [42]. The resulting Q^2-factor dependence versus signal power is shown in Fig. 11. The signal power is altered by increasing the imaginary part of the main spectrum, and in this particular configuration $a = \Im\lambda$. In Fig. 11, the performance of a noiseless transmission in a 1040 km fibre is also presented. A sharp decline in the Q^2-factor at high powers due to numerical errors is evident from this figure. This power-dependent numerical accuracy seems to be the leading contributor to the performance degradation after the optimum point in Fig. 11. The transmitted and received MPSK constellations are also shown in Fig. 12 for two different signal powers. In Fig. 12 (a) plotted at the point of optimum signal power, an error-free communication is

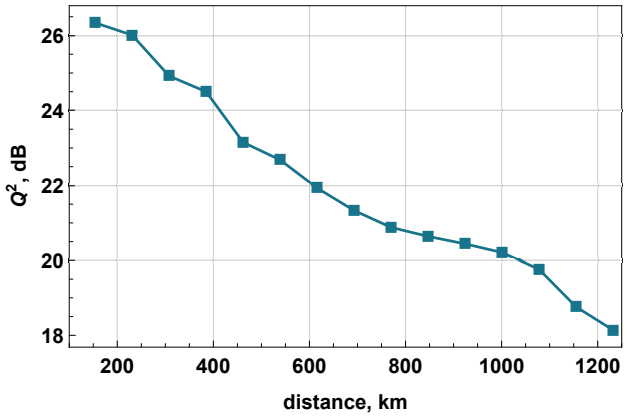

Fig. 13: The Q^2-factor versus transmission distance at optimum signal power $P = -17$ dBm.

provided up to the accuracy of our simulations. We note that the achievable Q-factor degrades with the propagation distance, see Fig. 13.

The average signal bandwidth is 9.8 GHz and the delivered data rate is 23.7 Gb/s up to 1040 km transmission, which shows a considerable improvement compared to our earlier work [21]. Here we also note that the highest data rate for the soliton-based QAM transmission system reported was ~ 24 Gb/s at 1000 km [37], so our proof-of-concept system here has already reached that value, which actually reveals the potential of the PNFT-based approaches. However, it has to be noted that the state-of-the-art NFT-based communication systems employing two polarisations and the so-called b-modulation concept, currently demonstrate much better efficiency numbers [43].

As we can observe in Fig. 12, there is a deterministic rotation in the phase domain even after the back-propagation stage performed by using Eq. (17). This phase rotation makes the received phases distribution asymmetric and can be remedied by means of a simple blind or, as we have implemented in this work, a pilot-aided equaliser which improves the performance up to 1.5 dBm. The length of the preamble is inconsiderable compared to the signal length.

In the end, we note that the spectral efficiency of the proposed system is still relatively small compared to other state-of-the-art optical communication systems, basically due to the large time-bandwidth product value per baud in our RHP-generated time-domain signals. This issue leaves the space for the further improvements of the concept and study of the other main NS structures that would yield better efficiency values.

VI. Discussion and Conclusion

In this work, for the first time, a complete inverse transformation method in the PNFT transmission system, based on the RHP solution, is used at the transmitter to generate the time domain signals starting from the specifically chosen NS containing our data. We developed a systematic way of modulating the parameters (basically, the phases) for periodic finite-band solutions to the NLSE, addressed the issue of exact periodicity for the carrier

wave-forms, and presented the approach for controlling the signal characteristics. We performed the analysis for the 23.7 Gb/s communication PNFT-based system addressing the transmission distances for up to 1000 km, proving the viability of the proposed concept. The favourable features of the PNFT and our RHP-based processing method, such as the ability to control the signal parameters (first of all, the duration), smaller processing window at the receiver, and lower DSP complexity, in addition to the large number of degrees of freedom made available by modulating the phases, lead to improved systems performance. The system's behaviour in terms of Q^2-factor vs. discretisation levels, distance and power, and BER numbers have been analysed. We also point out several possible ways of how to improve the performance of PNFT-based systems further, mentioning, in particular, the more involved structure of main spectrum, the use of 2π range for the phase modulation, the optimisation of sampling in both time and nonlinear spectral domains, and the utilisation of, e.g., pilots to get rid of deterministic offsets. Some other advancements may also include, e.g., the incorporation of improved Zakharov-Shabat solution methods at the receiver [44, 45], or some improved methods for solving the RHP numerically. Overall, based on the results obtained, we can assert that the proposed approach, though being so far in its rather nascent stage, allows us to gain a great flexibility, rectifying some drawbacks of "conventional" NFT systems and admitting further modification/improvements: it already reveals relatively deserving performance metrics, thus demonstrating its potential in achieving the high efficiency in optical communication systems' functioning.

Note added in proof. When this paper was under review, we became aware of the other group's work related to the PNFT-based optical transmission [46, 47]. Even though the other signal processing method based on algebro-geometric approach, was used there, and the solutions/parameters utilised for carrying the data were different, the viability of the PNFT-based optical transmission was also demonstrated in that work, including the experimental realisation of the concept.

VII. Acknowledgements

This work was supported by the Leverhulme Project RPG-2018-063, EPSRC (project TRANSNET, EP/R035342/1), and Erasmus+ mobility exchange programme. The two first authors, MK and AV, contributed equally to this work.

Appendix A
Relation between RHPs (8) and (6)

The solution $\hat{\mathbf{\Phi}}(t,z,\lambda)$ of the RHP (8), (9), where one sets $C_0^f = C_0^g = 0$, can be related to the solution $\mathbf{\Psi}(t,z,\lambda)$ of the RHP (5), (6) as follows [28]:

$$\begin{aligned}\hat{\mathbf{\Phi}}(t,z,\lambda) = &\exp\Big(i\left[f_0 t + g_0 z\right]\sigma_3\Big)\mathbf{\Psi}(t,z,\lambda)\\ &\times\exp\Big(-i\left[(f(\lambda)-\lambda)t + (g(\lambda)-2\lambda^2 z\right]\sigma_3\Big),\end{aligned} \tag{18}$$

where the functions $f(\lambda)$ and $g(\lambda)$ as well as f_0 and g_0 are determined by

$$f(\lambda) = \frac{w(\lambda)}{2\pi i}\sum_{j=1}^{\mathscr{N}}\int_{\Gamma_j}\frac{C_j^f d\xi}{w^+(\xi)(\xi-\lambda)} = \lambda + f_0 + O(\lambda^{-1}), \tag{19}$$

$$g(\lambda) = \frac{w(\lambda)}{2\pi i}\sum_{j=1}^{\mathscr{N}}\int_{\Gamma_j}\frac{C_j^g d\xi}{w^+(\xi)(\xi-\lambda)} = 2\lambda^2 + g_0 + O(\lambda^{-1}), \tag{20}$$

as $\lambda\to\infty$. In turn, C_j^f and C_j^g, $j=1,\dots,\mathscr{N}$, are determined as the unique solutions of systems of linear algebraic equations. Namely, if $\mathscr{N}\geq 3$, then $\mathbf{C}^f := [C_1^f,\dots,C_{\mathscr{N}}^f]^T$ and $\mathbf{C}^g := [C_1^g,\dots,C_{\mathscr{N}}^g]^T$ are the solutions of, respectively:

$$\mathbf{K}_1\mathbf{C}^f = \Big[\underbrace{0,\cdots,0}_{\mathscr{N}-1},-2\pi i\Big]^T, \tag{21}$$

$$\mathbf{K}_1\mathbf{C}^g = -4\pi i\Big[\underbrace{0,\cdots,0}_{\mathscr{N}-2},2,\sum_{j=0}^{\mathscr{N}}(\lambda_j+\lambda_j^*)\Big]^T, \tag{22}$$

where the $\mathscr{N}\times\mathscr{N}$ matrix $\mathbf{K}_1$ is expressed through $\mathbf{K}$ (14) with its first column and last row being taken out (for smaller $\mathscr{N}$, the r.h.s. in (21) and (22) are to be slightly modified [28]).

Appendix B
A procedure to find a main spectrum resulting in a periodic finite-gap solution

A. An iterative approach starting from a signal with infinitesimal power

Let Λ be a grid of equidistant points in the real direction having the same imaginary parts, see Fig. 2:

$$\Lambda = (-\lambda_{\mathscr{N}/2},\cdots,-\lambda_1,\lambda_0=0,\lambda_1=\Delta\lambda,\cdots,\lambda_{\mathscr{N}/2}). \tag{23}$$

This configuration is completely described by three parameters: $\Delta\Re\lambda$, $\mathscr{N}$ and $\Im\lambda\equiv a$. Let the main spectrum be Λ; then the contour integrals in Eqs. (21) become

$$\int_{\Gamma_j}\frac{\xi^k d\xi}{w(\xi)} = i\int_{-a}^{a}\frac{(\Re\lambda_j+it)^k dt}{w(\Re\lambda_j+it)}, \tag{24}$$

where

$$w_j(\lambda) = \prod_{\substack{i=-\mathscr{N}/2\\ i\neq j}}^{\mathscr{N}/2}\sqrt{(\lambda-\lambda_i)(\lambda-\lambda_i^*)}. \tag{25}$$

We have

$$\int_{\Gamma_j}\frac{\xi^k d\xi}{w(\xi)} = \int_{-a}^{a}\frac{(\Re\lambda_j+it)^k dt}{w_j(\Re\lambda_j+it)\sqrt{\Im\lambda_j^2-t^2}} \tag{26}$$

$$= 2\int_0^{\pi/2}\frac{(\Re\lambda_j+ia\sin x)^k dx}{w_j(\Re\lambda_j+ia\sin x)}\xrightarrow[a\to 0]{}\pi\frac{\lambda_j^k}{w_j(\lambda_j)}. \tag{27}$$

Eventually, we arrive at the values for the "frequencies" and "wave numbers" associated with an infinitesimal a:

$$C^f = -2\,(-\lambda_{\mathscr{N}/2},\cdots,-\lambda_1,\lambda_0=0,\lambda_1=\Delta\lambda,\cdots,\lambda_{\mathscr{N}/2}), \tag{28}$$

$$C_j^g = -\frac{(C_j^f)^2}{2}. \tag{29}$$

The last relation is nothing but the conventional square dispersion law for the NLSE. From Eq. (28) one can easily find a set of eigenvalues offering a commensurable vector C^f with the desired signal period (considering C_1^f) and signal bandwidth (considering $C_{\mathcal{N}}^f$). For the time duration (period) of the signal, T, we have $T = \frac{2\pi}{\min|C^f|}$, while the bandwidth is given by $BW = 2\pi\mathcal{N}\Delta\Re\lambda$.

For a finite, nonzero signal power, that corresponds to a finite, nonzero value of a, the main spectrum points have to be (numerically) readjusted: using Λ as the initial point, an optimisation problem is to be solved, where the main spectrum which renders the vector of C_j^fs closest to the desired values is to be reached.

B. Using a multi-carrier signal as a "billet" to find the signal with an appropriate main spectrum

As mentioned at the end of Sec. IV-B, it is the elements of C^f from Eq. (9) [assuming the carrier frequency $f_0 = 0$] that determine the periodicity of the signal, while signal's characteristics depend on the main spectrum structure. Moreover, in Sec. V-A we explained that the signal power is also predominantly determined by the main spectrum. In view of that, the main spectrum of an arbitrary periodic signal with the desired period and power can be used in constructing another periodic finite-gap signal: for doing this we take the main NS of the first and add up the modulated phases. Then we numerically construct the solution of the properly-defined respective RHP to recover the space-time profile for the signal containing our modulated data.

To illustrate the procedure depicted above, let us start with the multi-carrier signal $s_0(t)$:

$$s_0(t) = A\sum_{k=1}^{K} c_k \cos\omega_k t, \tag{30}$$

where K is the number of carriers, A is the power control parameter, and ω_k are the "linear" frequencies. Furthermore, let all c_k = const. By choosing $\omega_k = k\Delta\omega$, we can set the signal duration (period) to T_u by fixing $\Delta\omega = \frac{2\pi}{T_u}$. The signal bandwidth, on the other hand, is given by $BW = K\frac{\Delta\omega}{\pi}$, the value controllable by means of the free parameter K. The signal power than can be freely adjusted by altering A. So we construct the variant of the signal in Eq. (30) and numerically calculate its main spectrum. This main spectrum appended with modulated phases for each main spectrum point, is then used in the RHP solver to construct a periodic signal, $s_1(t)$, carrying our encoded data. s_1 has the same signal characteristics as those of the "billet" one, s_0. We emphasize, however, that $s_1(t)$ and $s_0(t)$ are not necessarily the same or even close to each other in their shape. In the way described above, the signal period and power independent of the auxiliary spectrum (see Sec. V-A), can be exactly predetermined. Moreover, at low signal powers, the imaginary part of the main spectrum of $s_1(t)$ approximates the linear spectrum of $s_0(t)$, see Fig. 14. As power increases, this approximation becomes less adequate, see Fig. 14. In Fig. 14, the linear spectrum of the periodic signal, $s_0(t)$, is depicted with a solid blue line connecting its values at discrete points for different signal powers while the imaginary part of the main spectrum of $s_0(t)$ is shown by the orange circles. This figure shows that at low powers, the imaginary part of the main spectrum resembles the amplitude of the linear spectrum of the signal.

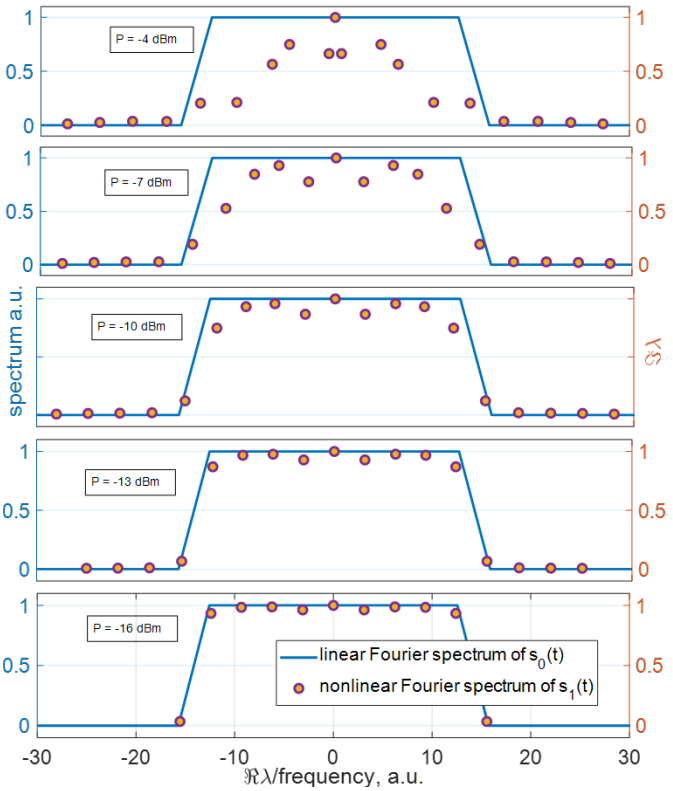

Fig. 14: Comparison of the linear Fourier spectrum of the multi-carrier signal $s_0(t)$ given by Eq. (30) and the main NS, as signal power decreases from the top $P = -4$ dBm to the bottom $P = -16$ dBm. We observe the clear convergence of the main spectrum to the linear Fourier transform of the multi-carrier signal. The x-axis represents the frequency for the linear spectrum and a properly scaled $\Re\lambda$ for the main spectrum.

REFERENCES

[1] V. Zakharov and A. Shabat, "Exact theory of two-dimensional self-focusing and one-dimensional self-modulation of waves in nonlinear media," *Soviet physics JETP*, vol. 34, no. 1, p. 62, 1972.

[2] A. Hasegawa and T. Nyu, "Eigenvalue communication," *Journal of Lightwave Technology*, vol. 11, no. 3, pp. 395–399, 1993.

[3] M. Yousefi and F. Kschischang, "Information transmission using the nonlinear Fourier transform, Part I: Mathematical tools," *IEEE Transactions on Information Theory*, vol. 60, no. 7, pp. 4312–4328, 2014.

[4] S. Turitsyn, J. Prilepsky, S. Le, S. Wahls, L. Frumin, M. Kamalian, and S. Derevyanko, "Nonlinear Fourier transform for optical data processing and transmis-

sion: advances and perspectives," *Optica*, vol. 4, no. 3, pp. 307–322, 2017.

[5] S. Le, V. Aref, and H. Buelow, "Nonlinear signal multiplexing for communication beyond the Kerr nonlinearity limit," *Nature Photonics*, vol. 11, no. 9, p. 570, 2017.

[6] S. Derevyanko, J. Prilepsky, and S. Turitsyn, "Capacity estimates for optical transmission based on the nonlinear Fourier transform," *Nature communications*, vol. 7, p. 12710, 2016.

[7] M. Kamalian, J. Prilepsky, S. Le, and S. Turitsyn, "Periodic nonlinear Fourier transform for fiber-optic communications, Part I: theory and numerical methods," *Optics express*, vol. 24, no. 16, pp. 18 353–18 369, 2016.

[8] M. Kamalian, A. Vasylchenkova, J. Prilepsky, D. Shepelsky, and S. Turitsyn, "Communication system based on periodic nonlinear fourier transform with exact inverse transformation," in *ECOC 2018; 44nd European Conference on Optical Communication; Proceedings of*, 2018, p. Tu3A.2.

[9] I. T. Lima, T. D. DeMenezes, V. S. Grigoryan, M. O'sullivan, and C. R. Menyuk, "Nonlinear compensation in optical communications systems with normal dispersion fibers using the nonlinear Fourier transform," *Journal of Lightwave Technology*, vol. 35, no. 23, pp. 5056–5068, 2017.

[10] S. Wahls, S. Chimmalgi, and P. J. Prins, "Wiener-Hopf method for b-modulation," in *Optical Fiber Communication Conference*. Optical Society of America, 2019, pp. W2A–50.

[11] M. Pankratova, A. Vasylchenkova, S. A. Derevyanko, N. B. Chichkov, and J. E. Prilepsky, "Signal-noise interaction in optical fiber communication systems employing nonlinear frequency division multiplexing," *submitted to Phys. Rev. Applied*, December 2019.

[12] S. Civelli, E. Forestieri, and M. Secondini, "Why noise and dispersion may seriously hamper nonlinear frequency-division multiplexing," *IEEE Photonics Technology Letters*, vol. 29, no. 16, pp. 1332–1335, 2017.

[13] S. Wahls and V. Vaibhav, "Fast inverse nonlinear Fourier transforms for continuous spectra of Zakharov-Shabat type," *arXiv preprint arXiv:1607.01305*, pp. 1–15, 2016.

[14] S. Wahls and V. Poor, "Fast numerical nonlinear Fourier transforms," *IEEE Transactions on Information Theory*, vol. 61, no. 12, pp. 6957–6974, 2015.

[15] S. Wahls, S. Chimmalgi, and P. J. Prins, "Wiener-Hopf method for b-modulation," in *2019 Optical Fiber Communications Conference and Exhibition (OFC)*. IEEE, 2019, pp. 1–3.

[16] J. G. Proakis and M. Salehi, *Digital communications*. McGraw-hill New York, 2001, vol. 4.

[17] M. Kamalian, S. Le, J. Prilepsky, and S. Turitsyn, "Statistical analysis of a communication system based on the periodic nonlinear Fourier transform," in *Australian Conference on Optical Fibre Technology*. Optical Society of America, 2016, pp. ATh1C–4.

[18] M. Kamalian, J. Prilepsky, A. Vasylchenkova, D. Shepelsky, and S. Turitsyn, "Methods of nonlinear Fourier-based optical transmission with periodically-extended signals," in *2018 IEEE International Conference on the Science of Electrical Engineering in Israel (ICSEE)*. IEEE, 2018, pp. 1–5.

[19] M. K. Kopae, J. E. Prilepsky, S. T. Le, and S. K. Turitsyn, "Optical communication based on the periodic nonlinear Fourier transform signal processing," in *2016 IEEE 6th International Conference on Photonics (ICP)*. IEEE, 2016, pp. 1–3.

[20] J.-W. Goossens, Y. Jaouën, and H. Hafermann, "Experimental demonstration of data transmission based on the exact inverse periodic nonlinear Fourier transform," in *Optical Fiber Communication Conference*. Optical Society of America, 2019, pp. M1I–6.

[21] M. Kamalian, A. Vasylchenkova, D. Shepelsky, J. Prilepsky, and S. Turitsyn, "Periodic nonlinear Fourier transform communication solving the Riemann-Hilbert problem," *J. Lightwave Technol.*, vol. 36, no. 24, pp. 5714–5727, 2018.

[22] M. Kamalian, J. Prilepsky, S. Le, and S. Turitsyn, "Periodic nonlinear Fourier transform for fiber-optic communications, part II: eigenvalue communication," *Optics Express*, vol. 24, no. 16, pp. 18 370–18 381, 2016.

[23] E. Belokolos, A. Bobenko, V. Enol'skii, A. Its, and V. Matveev, *Algebro-Geometric Approach to Nonlinear Integrable Equations*. Springer-Verlag, 1994.

[24] M. Kamalian, D. Shepelsky, A. Vasylchenkova, J. Prilepsky, and S. Turitsyn, "Communication system using periodic nonlinear Fourier transform based on Riemann-Hilbert problem," in *ECOC 2018; 44nd European Conference on Optical Communication; Proceedings of*, 2018, p. Tu3A.3.

[25] A. Arico, G. Rodriguez, and S. Seatzu, "Numerical solution of the nonlinear Schrödinger equation, starting from the scattering data," *Calcolo*, vol. 48, no. 1, pp. 75–88, 2011.

[26] G. Agrawal, *Nonlinear fiber optics*. Springer, 2000.

[27] M. Kamalian, J. Prilepsky, S. Le, and S. Turitsyn, "On the design of NFT-based communication systems with lumped amplification," *Journal of Lightwave Technology*, vol. 35, no. 24, pp. 5464–5472, 2017.

[28] V. Kotlyarov and D. Shepelsky, "Planar unmodular Baker-Akhiezer function for the nonlinear Schrödinger equation," *Annals of Mathematical Sciences and Applications*, vol. 2, no. 2, pp. 343–384, 2017.

[29] S. Olver, "A general framework for solving Riemann–Hilbert problems numerically," *Numerische Mathematik*, vol. 122, no. 2, pp. 305–340, 2012.

[30] T. Trogdon and S. Olver, "Numerical inverse scattering for the focusing and defocusing nonlinear Schrödinger equations," *Proceedings of the Royal Society A: Mathematical, Physical and Engineering Sciences*, vol. 469, no. 2149, p. 20120330, 2013.

[31] ——, *Riemann-Hilbert problems, their numerical solution, and the computation of nonlinear special functions*. SIAM, 2016.

[32] W. Q. Zhang, T. Gui, Q. Zhang, C. Lu, T. M. Monro,

T. H. Chan, A. P. T. Lau, and V. S. Afshar, "Correlated eigenvalues of multi-soliton optical communications," *Scientific reports*, vol. 9, no. 1, p. 6399, 2019.

[33] O. Kotlyar, M. Pankratova, M. Kamalian, A. Vasylchenkova, J. E. Prilepsky, and S. K. Turitsyn, "Unsupervised and supervised machine learning for performance improvement of NFT optical transmission," in *2018 IEEE British and Irish Conference on Optics and Photonics (BICOP)*, 2018, pp. 1–4.

[34] M. Kamalian-Kopae, A. Vasylchenkova, O. Kotlyar, M. Pankratova, J. Prilepsky, and S. Turitsyn, "Artificial neural network-based equaliser in the nonlinear Fourier domain for fibre-optic communication applications," in *2019 Conference on Lasers and Electro-Optics Europe European Quantum Electronics Conference (CLEO/Europe-EQEC)*, June 2019.

[35] O. Kotlyar, M. Kamalian Kopae, J. E. Prilepsky, M. Pankratova, and S. K. Turitsyn, "Machine learning for performance improvement of periodic NFT-based communication system," in *2019 European Conference on Optical Communications*, 2019.

[36] M. Kamalian, J. Prilepsky, S. Derevyanko, S. Le, and S. Turitsyn, "Nonlinear fourier based spectral filtering," in *Lasers and Electro-Optics (CLEO), Conference on*. IEEE, 2017.

[37] T. Gui, C. Lu, A. P. T. Lau, and P. Wai, "High-order modulation on a single discrete eigenvalue for optical communications based on nonlinear Fourier transform," *Optics Express*, vol. 25, no. 17, pp. 20 286–20 297, 2017.

[38] S. Civelli, L. Barletti, and M. Secondini, "Numerical methods for the inverse nonlinear fourier transform," in *2015 Tyrrhenian International Workshop on Digital Communications (TIWDC)*, Sep. 2015, pp. 13–16.

[39] M. Yousefi and F. Kschischang, "Information transmission using the nonlinear Fourier transform, Part III: Spectrum modulation," *IEEE Transactions on Information Theory*, vol. 60, no. 7, pp. 4346–4369, 2014.

[40] E. Tracy and H. Chen, "Nonlinear self-modulation: An exactly solvable model," *Physical Review A*, vol. 37, no. 3, pp. 815–839, 1988.

[41] K. T. McLaughlin and P. V. Nabelek, "A Riemann–Hilbert problem approach to periodic infinite gap Hill operators and the Korteweg–de Vries equation," *arXiv preprint arXiv:1810.07818*, 2018.

[42] M. Kamalian Kopae, "On nonlinear fourier transform-based fibre-optic communication systems for periodic signals," Ph.D. dissertation, Aston University, 2018.

[43] X. Yangzhang, V. Aref, S. T. Le, H. Buelow, D. Lavery, and P. Bayvel, "Dual-polarization non-linear frequency-division multiplexed transmission with b-modulation," *Journal of Lightwave Technology*, vol. 37, no. 6, pp. 1570–1578, 2019.

[44] S. Chimmalgi, P. J. Prins, and S. Wahls, "Nonlinear Fourier transform algorithm using a higher order exponential integrator," in *Advanced Photonics 2018*. Optical Society of America, 2018, p. SpM4G.5.

[45] S. Medvedev, I. Vaseva, I. Chekhovskoy, and M. Fedoruk, "Numerical algorithm with fourth-order accuracy for the direct Zakharov-Shabat problem," *Optics letters*, vol. 44, no. 9, pp. 2264–2267, 2019.

[46] J.-W. Goossens, H. Hafermann, and Y. Jaouën, "Data transmission based on exact inverse periodic nonlinear Fourier transform, Part I: Theory," *arXiv preprint arXiv:1911.12614*, 2019.

[47] ——, "Data transmission based on exact inverse periodic nonlinear Fourier transform, Part II: Waveform design and experiment," *arXiv preprint arXiv:1911.12615*, 2019.